Predictions and measurements of sound transmission through a periodic array of elastic shells in air

Anton Krynkin[a] and Olga Umnova
Acoustics Research Centre, The University of Salford, Salford, Greater Manchester, United Kingdom

Alvin Yung Boon Chong, Shahram Taherzadeh, and Keith Attenborough
Department of Design Development Environment and Materials, The Open University, Milton Keynes, United Kingdom

Analytical and numerical approaches have been made to the problems of (a) propagation through a doubly periodic array of elastic shells in air, (b) scattering by a single elastic shell in air, and (c) scattering by a finite periodic array of elastic shells in air. Using the Rayleigh identity and the Kirchhoff–Love approximations, a relationship is found between the elastic material parameters and the size of the bandgap below the first Bragg frequency, which results from the axisymmetric resonance of the shells in an array. Predictions and laboratory data confirm that use of a suitably "soft" non-vulcanized rubber results in substantial insertion loss peaks related to the resonances of the shells. Inclusion of viscoelasticity is found to improve the correspondence between predictions and data. In addition the possible influences of inhomogeneity due to the manufacturing of the elastic shells (i.e., the effects of gluing sheet edges together) and of departures from circular cylindrical cross-sections are considered by means of numerical methods.
© 2010 Acoustical Society of America. [DOI: 10.1121/1.3506342]

I. INTRODUCTION

Periodic arrays of circular cylinders are known to give high attenuation at selective frequencies as a consequence of Bragg scattering.[1,2] They give rise to bandgaps, i.e., peaks in transmission loss, related to the spacing between scattering elements (the lattice constant). The first bandgap central frequency occurs when the lattice constant is equal to half wavelength. Such arrays have been dubbed "sonic crystals" (SCs) or "phononic crystals" because of the analogous effects to those of photonic crystals on electromagnetic waves. By varying the lattice constant and/or filling fraction it is possible to attain peaks of attenuation in a certain range of frequencies. Potentially, barriers made in the form of periodic cylinder arrays will be more esthetically pleasing than conventional noise barriers and their performance might be less affected by wind.

For SCs to be useful as sound barriers, methods must be found of reducing the angle-dependence of the stop bands and targeting the noise spectrum of interest. One possibility for achieving a relatively low-frequency angle-independent stop band is to use resonant scatterers. There has been previous numerical and theoretical work in respect of periodic arrays of elastic scatterers in a gas involving hollow spheres and cylinders.[3] There have also been numerical studies of the acoustical performance of a periodic array of resonant silicone rubber scatterers embedded in an epoxy resin matrix.[4] Previous laboratory work in respect of periodic arrays of scatterers in air has investigated the use of pressurized gas-filled cylindrical balloons.[5,6] However it was found difficult to predict the measured effects. Indeed it is essential to introduce the effect of any static external load to model scattering by elastic materials under tension. Another form of resonant scatterer is a cylinder with a slit along its length.[7] Recent studies[8] suggest the possibility of using hollow tubes with multiple narrow slits, such that all the slits occupy the quadrants facing the source, to create a broader bandgap.

In this paper, first the theory of wave propagation through doubly periodic arrays of elastic shells is developed. A new result compared with previous work is a semi-analytical approximation for thin "soft" elastic shells. It is assumed that the elastic material is called soft, if $c_2/c_1 \ll 1$, where c_1 and c_2 are the compressional and shear wave speeds, respectively. The properties of this material allow several relatively low-frequency resonances that generate stop bands in the scattering problem for array. These stop bands are additional to those related to the wave propagation through the array of rigid/porous scatterers.[2] In the experiments and predictions reported here, commercially available non-vulcanized rubber (latex) is used as an example of a suitable material. Using the approximation results, the scattering problem is solved for a single scatterer and for a finite array of scatterers. Comparisons with data confirm the presence of the interesting resonances for the chosen material and geometry of the shell.

II. ANALYTICAL AND NUMERICAL RESULTS

A. Doubly periodic array of elastic shells: Formulation

First consider the problem of acoustic wave propagation through a doubly periodic array of identical elastic shells. Throughout the paper the time-harmonic dependence is taken

---

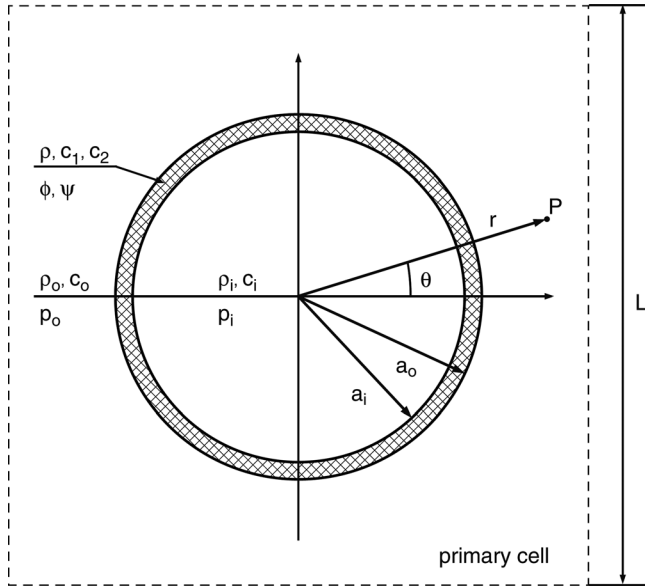[a] Author to whom correspondence should be addressed. Electronic mail: a.krynkin@salford.ac.uk

FIG. 1. Cross-section of an elastic shell in the primary cell of doubly periodic array.

as $\exp(-i\omega t)$. It is assumed that waves propagate in the plane perpendicular to the main axis of infinite cylindrical shells C_j, j takes positive integer values, so each shell can be replaced by its cross-section (i.e., elastic ring), see Fig. 1. The acoustic environment outside/inside of each shell is described by density ρ_o/ρ_i and sound speed c_o/c_i, whereas the elastic linear isotropic material of the shell is represented by density ρ, compressional velocity c_1, and shear velocity c_2.

Without loss of generality, the origins of the Cartesian (x, y) and polar coordinates (r, θ) used in this section coincide with the center of the scatterer C_0 in the primary cell of size L, referred to as the lattice constant. Center O_j of each scatterer in the infinite periodic array is defined by the position vector $R_j = n_1\mathbf{a}_1 + n_2\mathbf{a}_2$; n_1, n_2 take integer values, where $\mathbf{a_1}$ and $\mathbf{a_2}$ are the fundamental translation vectors.[9]

Displacement potential $p(\mathbf{r})$ in the acoustic medium satisfies the Helmholtz equation,

$$\Delta p + k_\alpha^2 p = 0, \tag{1}$$

and the quasi-periodicity conditions,

$$p(\mathbf{r} + \mathbf{R}_j) = \exp(i\beta^T \mathbf{R}_j)p(\mathbf{r}), \tag{2}$$

where $\Delta = (1/r)(\partial/\partial r)(r\partial/\partial r) + (1/r^2)(\partial^2/\partial\theta^2)$, $k_\alpha = \omega/c_\alpha$ is the wavenumber defined as the ratio between angular frequency ω and sound speed of the outer acoustic environment c_α, $\beta = (q_1, q_2)^T$ is a given wave vector, and index α relates density to one of the acoustic media (i.e., it equals to either "o" or "i"). $p(\mathbf{r})$ is related to the acoustic pressure $\Phi(\mathbf{r})$ and particle velocity potential $\hat{\Phi}(\mathbf{r})$ by

$$\Phi = \rho_\alpha \omega^2 p, \tag{3a}$$

$$\hat{\Phi} = -i\omega p. \tag{3b}$$

The wave field in the elastic ring is represented by two displacement potentials $\phi(\mathbf{r})$ and $\psi(\mathbf{r})$, which are solutions of the following equations:[10]

$$\Delta\phi + k_1^2\phi = 0, \tag{4a}$$

$$\Delta\psi + k_2^2\psi = 0, \tag{4b}$$

where $k_1 = \omega/c_1$ and $k_2 = \omega/c_2$.

The solutions to Eqs. (1) and (4) are subject to continuity conditions at the elastic–acoustic interface of scatterer C_j. This gives at $r = a_o$ and $r = a_i$,

$$\sigma_{rr} = -\rho_\alpha \omega^2 p, \tag{5a}$$

$$\sigma_{r\theta} = 0, \tag{5b}$$

$$\frac{\partial p}{\partial r} = \frac{\partial \phi}{\partial r} + \frac{1}{r}\frac{\partial \psi}{\partial \theta}, \tag{5c}$$

where stresses σ_{rr} and $\sigma_{r\theta}$ are defined by

$$\sigma_{rr} = \frac{2\rho c_2^2}{r^2}\left[\frac{\partial}{\partial\theta}\left(r\frac{\partial\psi}{\partial r} - \psi\right) - \left(r\frac{\partial\phi}{\partial r} + \frac{\partial^2\phi}{\partial\theta^2}\right)\right] - \rho\omega^2\phi, \tag{6a}$$

$$\sigma_{r\theta} = \frac{2\rho c_2^2}{r^2}\left[\frac{\partial}{\partial\theta}\left(r\frac{\partial\phi}{\partial r} - \phi\right) + r\frac{\partial\psi}{\partial r} + \frac{\partial^2\psi}{\partial\theta^2}\right] + \rho\omega^2\psi. \tag{6b}$$

The solutions to the problems (1)–(5) can be described by orthogonal series of Bessel and trigonometric functions. In the outer and inner acoustic media the potentials take the following forms:

$$p_o(r, \theta) = \sum_{n=-\infty}^{+\infty} [A_n J_n(k_o r) + B_n Y_n(k_o r)]$$
$$\times \exp(in\theta), \qquad r > a_o, \tag{7a}$$

$$p_i(r, \theta) = \sum_{n=-\infty}^{+\infty} E_n J_n(k_i r)\exp(in\theta), \qquad r < a_i, \tag{7b}$$

whereas the solutions of the elastic shell are expanded as

$$\phi(r, \theta) = \sum_{n=-\infty}^{+\infty}\left[C_{1,n}J_n(k_1 r) + C_{2,n}Y_n(k_1 r)\right]$$
$$\times \exp(in\theta), \qquad a_i < r < a_o, \tag{8a}$$

$$\psi(r, \theta) = \sum_{n=-\infty}^{+\infty}\left[D_{1,n}J_n(k_2 r) + D_{2,n}Y_n(k_2 r)\right]$$
$$\times \exp(in\theta), \qquad a_i < r < a_o. \tag{8b}$$

The set of unknown coefficients $\{A_n, C_{1,n}, C_{2,n}, D_{1,n}, D_{2,n}, E_n\}$ can be identified in terms of coefficient B_n by using boundary conditions at the surface of the elastic shell. Thus, substituting solutions of Eqs. (7) and (8) into Eq. (5) and

taking inner product $\int_0^{2\pi}\langle\cdot\rangle\exp(im\theta)d\theta$ one can derive an algebraic system of equations,

$$A_n = \frac{\left[a_o J_n'(k_o a_o),\, i\,n\,J_n(k_o a_o),\, a_o Y_n'(k_o a_o),\, i\,n\,Y_n(k_o a_o)\right]\mathbf{X}_n}{a_o J_n'(k_o a_o)}$$
$$-\frac{Y_n'(k_o a_o)}{J_n'(k_o a_o)}B_n, \tag{9}$$

$$\mathcal{C}_n\mathbf{X}_n = \left[0, 0, -\frac{2\kappa_o\epsilon_o k_o^2}{a_o\pi J_n'(k_o a_o)}, 0\right]^T B_n, \tag{10}$$

where $-\infty < n < \infty$, $\kappa_\alpha = c_\alpha/c_2$, $\epsilon_\alpha = \rho_\alpha c_\alpha/(\rho c_2)$, and $Z_n'(k_\alpha r) = dZ_n(k_\alpha r)/dr$ is the derivative of cylindrical function, $\mathbf{X}_n$ is the vector $(C_{1,n}, D_{1,n}, C_{2,n}, D_{2,n})^T$ of unknown coefficients, and $\mathcal{C}_n$ is the matrix of 4×4 elements in the following form:

$$\mathcal{C}_n = \begin{pmatrix} f_{1,i,J} & f_{2,i,J} & f_{1,i,Y} & f_{2,i,Y} \\ g_{1,i,J} & g_{2,i,J} & g_{1,i,Y} & g_{2,i,Y} \\ f_{1,o,J} & f_{2,o,J} & f_{1,o,Y} & f_{2,o,Y} \\ g_{1,o,J} & g_{2,o,J} & g_{1,o,Y} & g_{2,o,Y} \end{pmatrix}, \tag{11}$$

where the coefficients are defined as

$$f_{1,\alpha,Z} = \left[-\frac{2}{a_\alpha} + \frac{\epsilon_\alpha\kappa_\alpha k_\alpha^2 Z_n(k_\alpha a_\alpha)}{Z_n'(k_\alpha a_\alpha)}\right]Z_n'(k_1 a_\alpha)$$
$$+\frac{2n^2 - k_2^2 a_\alpha^2}{a_\alpha^2}Z_n(k_1 a_\alpha), \tag{12a}$$

$$f_{2,\alpha,Z} = \frac{in}{a_\alpha}\left\{2Z_n'(k_2 a_\alpha) + \left[-\frac{2}{a_\alpha} + \frac{\epsilon_\alpha\kappa_\alpha k_\alpha^2 Z_n(k_\alpha a_\alpha)}{Z_n'(k_\alpha a_\alpha)}\right]\right.$$
$$\left.\times Z_n(k_2 a_\alpha)\right\}, \tag{12b}$$

$$g_{1,\alpha,Z} = \frac{2\,in}{a_\alpha}\left[Z_n'(k_1 a_\alpha) - \frac{Z_n(k_1 a_\alpha)}{a_\alpha}\right], \tag{12c}$$

$$g_{2,\alpha,Z} = \frac{1}{a_\alpha}\left[2Z_n'(k_2 a_\alpha) - \frac{2n^2 - k_2^2 a_\alpha^2}{a_\alpha}Z_n(k_2 a_\alpha)\right]. \tag{12d}$$

In the case of the rigid scatterer Eq. (9) is reduced to the well-known relation between coefficients A_n and B_n by setting $\mathbf{X}_n$ to the zero vector and ε_o to the zero value.

The periodicity condition (2) can now be used to establish the dispersion relation in the form of the Rayleigh identity[11,12] for solution of the wave propagation problems (1)–(5), yielding

$$A_n = \sum_{m=-\infty}^{+\infty}(-1)^{m-n}\sigma_{m-n}(k_o, \beta)B_m, \quad -\infty < n < \infty. \tag{13}$$

Equation (13) involves the lattice sum,

$$\sigma_n(k_o, \beta) = \sum_{R_j\in\Lambda\backslash\{\mathbf{0}\}}\exp(i\beta^T\mathbf{R}_j)Y_n(k_o R_j)\exp(in\alpha_j),$$
$$-\infty < n < \infty, \tag{14}$$

within which Λ is the lattice where scatterers are distributed and position vector $\mathbf{R}_j$ is defined as $R_j(\cos\alpha_j, \sin\alpha_j)^T$. It must be noted that convergence of infinite sum in Eq. (14) can be improved by transforming it to the sum over the reciprocal lattice Λ^* (Ref. 12).

Substitution of Eqs. (9) and (10) into relation (13) gives

$$M_n B_n + \sum_{m=-\infty}^{+\infty}(-1)^{m-n}\sigma_{m-n}(k_o, \beta)B_m = 0,$$
$$-\infty < n < \infty, \tag{15}$$

where the coefficients M_n obtained from Eq. (9) characterize the type of the circular scatterer and the boundary conditions imposed on its surface.[13] In the limiting case when the continuity boundary conditions (5) are replaced by the Neumann conditions $\partial p/\partial r = 0$ (i.e., for a rigid scatterer) one can find that

$$M_n = \frac{Y_n'(k_o a_o)}{J_n'(k_o a_o)}. \tag{16}$$

The solutions are obtained by finding zeros of the determinant based on the coefficients matrix of algebraic set of equations (15). These solutions represent the dependence of the frequency parameter k_o on the wave vector β. Note that throughout the paper this wave vector is limited to contour $\Gamma MK\Gamma$ also known as first irreducible Brillouin zone. The nodes of the contour are defined as follows: $\Gamma = (0, 0)$, $M = (\pi, 0)$, and $K = (\pi, \pi)$.

The predictions in Fig. 2 illustrate the existence of propagating waves for different types of scatterers. The results show the difference between rigid and elastic scatterers. In particular, the result highlighted in the shaded area of Fig. 2(b) proves the fact that the array of soft elastic shells (latex in our case) may support a low-frequency complete bandgap characterized by the breathing mode resonance of an elastic shell in air. The resonance generates a standing wave in the infinite periodic array that creates the lower bound of the gap. This gap where waves do not propagate is observed below the first bandgap associated with the periodic arrangement normally called the Bragg bandgap. The latter characterizes the typical behavior of the doubly periodic array of rigid scatterers shown in Fig. 2(a). Note that the first Bragg bandgap exists around the pole $kL = \pi$ of the lattice sum $\sigma_n(k, \beta)$, n takes integer values.

Since the surrounding acoustic environment is assumed to be always the same (in this paper, it is air with $\rho_o = \rho_i = 1.25$ kg/m^3 and $c_o = c_i = 344$ m/s), it is clear that the position of resonance only depends on the shell radius a_o, half-thickness h, and the shell material parameters such as density, Young's modulus E, and Poisson's ratio v. Thus, our main interest is to find the range of shell properties that will ensure that the bandgap related to a shell resonance appears below the first Bragg bandgap.

B. Approximations for loaded thin elastic shell

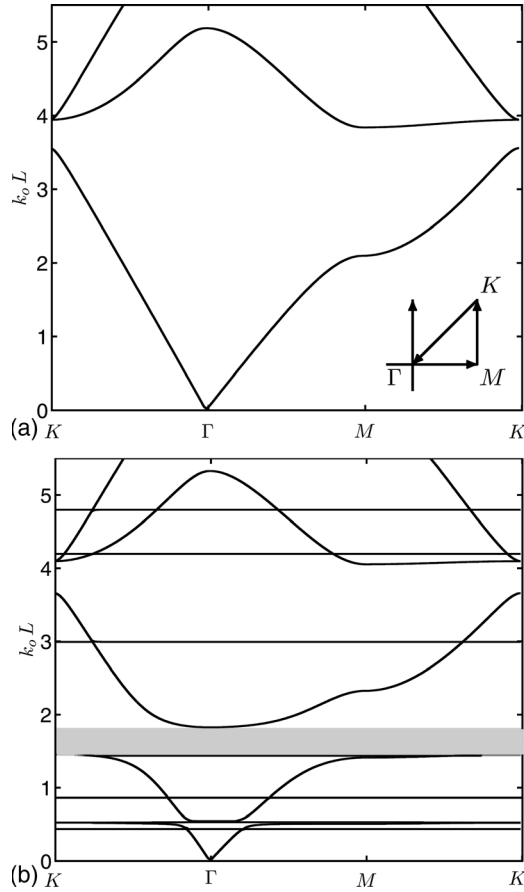The small thickness, low-frequency regime defined here as $\omega h/c_2 \ll 1$, and the considerable contrast between

FIG. 2. Solutions of Eq. (15) along the contour $\Gamma M K \Gamma$. The periodic arrays have lattice constant $L = 0.08$ m. (a) Periodic array of rigid scatterers of radius $a_o = 0.0275$ m. (b) Periodic array of elastic shells of radius $a_o = 0.0275$ m, thickness $2h = 0.00025$ m, density $\rho = 1100$ kg/m³, $c_1 = 954$ m/s, and $c_2 = 23$ m/s.

acoustic and elastic material parameters can be exploited to find the relation between the position of the Bragg bandgap and shell resonances.

If the thickness of the elastic shell is much smaller than its mid-surface radius $R = (a_o + a_i)/2$, then $\eta = h/R \ll 1$. On the other hand the contrast between elastic material of the shell and air medium considered here is relatively large. This can be described in terms of the relative impedance $\epsilon = \rho_o c_o/(\rho c_2) \ll 1$. To have better interaction between elastic and acoustic media, the contrast has to be reduced. The latter can be achieved by assuming that the relative impedance is of the same order as the ratio between half-thickness and mid-surface radius of the elastic shell. This can be written as

$$\epsilon \sim \eta. \qquad (17)$$

Based on the previously detailed assumptions concerning the thickness and relative impedance, one can derive long-wave low-frequency approximations for the wave equations of the thin-walled elastic shell following the technique described elsewhere.[14] Then the problem stated by Eq. (4) and boundary conditions (5a)–(5c) can be reduced to the asymptotic equations given by

$$\frac{1}{R^2}\left(\frac{\partial u_2}{\partial \theta} + u_1\right) - k_3^2 u_1 = -\frac{\epsilon}{\kappa_o}\frac{k_3^2[p_o(R,\theta) - p_i(R,\theta)]}{2h},$$
$$(18a)$$

$$\frac{1}{R^2}\left(\frac{\partial^2 u_2}{\partial \theta^2} + \frac{\partial u_1}{\partial \theta}\right) + k_3^2 u_2 = 0, \qquad (18b)$$

where $u_1(\theta)$ and $u_2(\theta)$ are the approximations of the in-plane displacement components in the elastic shell, $k_3 = \omega/c_3$ and $\kappa_o = c_o/c_2$. Here the dilatational wave speed c_3 for a thin elastic plate is recalled,

$$c_3 = \sqrt{\frac{E}{\rho(1-v^2)}}. \qquad (19)$$

The right-hand sides of Eq. (18) describe the type of surface loading applied to the walls of the shell. In our case only the membrane compression form of loading can be observed.[14]

Equations (18a) and (18b) are solved in conjunction with the conditions imposed on the displacements at the shell mid-surface that are

$$\left.\frac{\partial p_o(r,\theta)}{\partial r}\right|_{r=R} = \left.\frac{\partial p_i(r,\theta)}{\partial r}\right|_{r=R}, \qquad (20a)$$

$$\left.\frac{\partial p_o(r,\theta)}{\partial r}\right|_{r=R} = u_1(\theta). \qquad (20b)$$

The displacements of the elastic shell can be expanded into the Fourier series,

$$u_1(\theta) = \sum_{n=-\infty}^{+\infty} U_{1,n} \exp(in\theta), \qquad (21a)$$

$$u_2(\theta) = \sum_{n=-\infty}^{+\infty} U_{2,n} \exp(in\theta), \qquad (21b)$$

whereas acoustic potentials may take the same form as in relations (7a) and (7b) if wave propagation through the periodic array of thin elastic shells is studied. Inserting acoustic and elastic components into Eqs. (18) and (20) one can derive an approximation for coefficients M_n, yielding

$$M_n = \frac{Y_n'(k_o R)}{J_n'(k_o R)}\left[1 + \frac{\hat{U}_{1,n}}{Y_n'(k_o R)}\right], \qquad (22)$$

where

$$\hat{U}_{1,n} = \frac{\epsilon}{\kappa_o}\frac{n^2 - k_3^2 R^2}{\pi R h\left(1 + n^2 - k_3^2 R^2\right)J_n'(k_o R)}. \qquad (23)$$

It is noted that as $\epsilon \to 0$ the given form of M_n transforms to the coefficient for the rigid scatterer (16).

The results can be compared with the exact form of coefficient M_n derived from Eqs. (9) and (10). Figure 3(a) demonstrates that the approximation is within 1% of the exact solution for the modes related to a rigid shell and to the first elastic shell resonances of different indices. Also, two major bandgaps below the first Bragg bandgap are predicted. They can be identified with the two elastic shell resonances with indices $n = 0$ and $n = \pm 1$ as shown by the predictions in Fig. 3(b). The predictions in Fig. 3(b) are
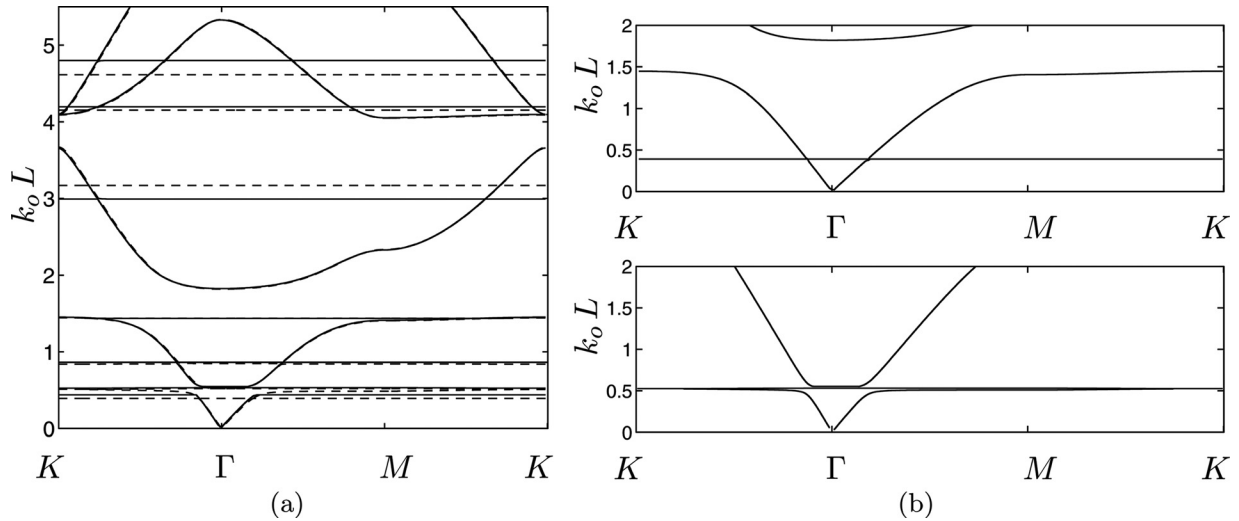
FIG. 3. The eigenvalue solution along the contour $\Gamma MK\Gamma$ for the periodic array of thin elastic shells of radius $a_o = 0.0275$ m and thickness $2h = 0.00025$ m with lattice constant $L = 0.08$ m. The material parameters of the shell are $\rho = 1100$ kg/m^3, $c_1 = 954$ m/s, and $c_2 = 23$ m/s corresponding to $E \approx 1.75$ MPa and $v \approx 0.4997$. (a) (——) Solutions of Eq. (15) compared with (- - -), the shell approximations (18). (b) Only the two different types of shell resonances are allowed in the calculations. The upper graph is associated with $n = 0$ resonance and the lower graph corresponds to $n = \pm 1$ resonance.

obtained by allowing coefficient M_n only to take form (22) for the specified indices while for all other values it is given in the form for the rigid scatterer coefficient (16). There is also a third resonance related to $n = \pm 2$, which appears at $kL \approx 0.86$. The bandgap for this resonance is predicted to be almost negligible. Nevertheless this bandgap is observed clearly in the laboratory experiments described in Sec. III C. Reasons for this are discussed later.

The bandgap for $n = 0$ is a result of the axisymmetric resonance of the shell, since it does not depend on polar angle θ. To estimate the lower bound of this gap the resonance of the single shell has to be found. This requires solution of the appropriate eigenvalue problem, where the outer acoustic potential is given by the Bessel function of second kind only and the displacement field in the shell obeys Eq. (18). The solution of this problem corresponds to zeros of determinant of the coefficient matrix. The determinant takes form of the expression found in the square brackets of relation (22), which can be approximated by introducing a new small parameter. This parameter is based on the assumption that the radius of the elastic shell is much smaller than wavelength in air (i.e., $k_o R \ll 1$).

Expanding Bessel functions and collecting similar orders of smallness in accordance with Eq. (17) results in the leading order approximation, yielding

$$8\eta\left[4(\kappa^2 - 1) + \kappa_o^2(kR)^2\right]$$
$$+ \epsilon\kappa_o\left[(kR)^2\left(4\log\frac{2}{kR} - 4\gamma + 1\right) - 8\right] = 0, \quad \text{as} \quad kR \to 0,$$
(24)

where $\kappa = c_2/c_1$, and $\gamma \approx 0.5772$ is the Euler's constant.[15] Solution of this equation gives the critical value of the lower bound of the corresponding bandgap. For example, for a latex shell of radius $a_o = 0.0275$ m, thickness $2h = 0.00025$ m, density $\rho = 1100$ kg/m^3, wave velocities $c_1 = 954$ m/s, and $c_2 = 23$ m/s, the first solution of Eq. (24) is found at $kL \approx 1.42$.

The resonant frequency of the latex calculated from approximate equation (24) deviates by no more than 2% from the exact solution given by zeros of Eq. (22). By lowering the approximation accuracy to 6% the relation (24) can be reduced to a simple quadratic equation from which the resonance of the elastic shell in air can be found explicitly, i.e.,

$$(kR)^2 = \frac{1}{\eta\kappa_o^2}\left[4\eta(1 - \kappa^2) + \epsilon\kappa_o\right], \quad \text{as} \quad kR \to 0. \quad (25)$$

A more detailed analysis of how size and position of the bandgap vary with respect to material parameters is illustrated in Fig. 4, where the lower bound is approximated by roots of Eq. (24) and the upper bound is the solution of Rayleigh identity, Eq. (15). The results show that to have relatively large bandgap in an interesting frequency interval, the material contrast at the acoustic–elastic interface has to be reduced to minimum.
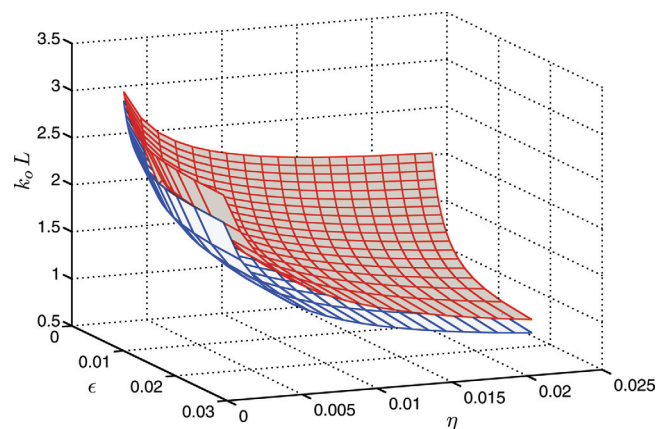

FIG. 4. (Color online) Size and position of the bandgap characterized by the axisymmetric resonance of the thin elastic shell. The solution in terms of scaled frequency k_oL is plotted against two dimensionless parameters ϵ and $\eta = h/R$ with $R = 0.027625$ m. Upper and lower surfaces correspond to the upper and lower bounds of the gap.

Krynkin *et al.*: Periodic array of elastic shells

C. Auxiliary problem: Single elastic shell

The efficiency of the approximations can be explored further by comparing predictions of the solution of the auxiliary scattering problem for a single shell with the data. We consider a two-dimensional (2D) problem consisting of a single thin elastic shell surrounded by an acoustic medium. The relative impedance obeys condition (17). Acoustic waves are generated by a cylindrical source, which is positioned in the outer region of the shell. The origin of the Cartesian (x, y) and polar coordinates (r, θ) coincides with the source location.

Potential $p_o(\boldsymbol{r})$ in the outer acoustic medium satisfies the Helmholtz equation (1) and Sommerfeld's radiation conditions,

$$\frac{\partial p_o}{\partial r} - ikp_o = o\left(r^{-1/2}\right), \quad \text{as} \quad r \to \infty, \tag{26}$$

where $r = \sqrt{x^2 + y^2}$. The solution representing scattered field is given by

$$p_{o,s}(r, \theta) = \sum_{n=-\infty}^{+\infty} A_n Z_n H_n^{(1)}(k_o \hat{r}) \exp(in\hat{\theta}), \quad \hat{r} > a_o, \tag{27}$$

so that total field in the outer acoustic medium takes the following form:

$$p_o(r, \theta) = H_0^{(1)}(k_o r) + p_{o,s}(r, \theta), \tag{28}$$

where $\hat{r}(r, \theta)$ and $\hat{\theta}(r, \theta)$ are the polar coordinates of receiver with origin placed at the center of scatterer, A_n are unknown coefficients and factors Z_n are found from

$$Z_n = \frac{J_n'(k_o R)}{H_n^{(1)'}(k_o R) + i\hat{U}_{1,n}}. \tag{29}$$

Note that when $\hat{U}_{1,n} = 0$ factors Z_n transform to those for the case of a rigid cylinder.

Use of the formulations from Secs. II A and II B leads to solutions for the inner acoustic medium and thin shell as relations (7) and (21), respectively. Note that for future use the cylindrical source function in Eq. (28) has to be expanded into series using Graf's addition theorem so that only one set of polar coordinates is employed. This gives

$$p_o(\hat{r}, \hat{\theta}) = \sum_{n=-\infty}^{+\infty} \left\{ J_n(k_o \hat{r}) H_n^{(1)}(k_o Q) \exp[-in(\pi + \alpha)] \right.$$
$$\left. + A_n Z_n H_n^{(1)}(k_o \hat{r}) \right\} \exp(in\hat{\theta}), \quad \hat{r} > a_o, \tag{30}$$

within which vector $\boldsymbol{Q} = Q(\cos\alpha, \sin\alpha)$ is the radius vector to the center of shell.

The unknown coefficients can be derived by using asymptotic equations (18a) and (18b), boundary conditions (20a) and (20b), and the modified solution (30). After solving the appropriate algebraic system, coefficients A_n are derived as

$$A_n = -H_n^{(1)}(k_o Q) \exp[-in(\pi + \alpha)], \quad -\infty < n < \infty. \tag{31}$$

The formulation outlined here describes wave scattering from a thin shell made of a perfectly elastic material. According to the results of Sec. II B, interesting effects are observed for so-called soft elastic materials that can be identified by $c_2/c_1 \ll 1$. Relevant viscoelasticity has to be taken into account. For rubber-like solids, viscoelasticity can be described by a linear model. The dynamic Young's modulus is[16]

$$E(t) = \hat{E}[1 - f(t)], \tag{32}$$

within which we introduce dynamic Young's modulus $\hat{E}$ and relaxation function of the following well-known form:

$$f(t) = \sum_j \hat{E}_j[1 - \exp(-t/\tau_j)], \tag{33}$$

where the sum of measured extensional moduli $\hat{E}_j$ is taken over relaxation times τ_j.

Applying the Laplace transform $\int_0^{+\infty}\langle\cdot\rangle\exp(-st)dt$, one can derive the Young's modulus in terms of the transform parameter s as

$$E(s) = \hat{E}[1 - sF(s)], \tag{34a}$$

$$F(s) = \sum_j \frac{\hat{E}_j}{s(1 + s\tau_j)}. \tag{34b}$$

This can also be represented in the frequency domain by using $s = -i\omega$, so that

$$E(\omega) = \hat{E}\left[1 - \sum_j \frac{\hat{E}_j}{(1 - i\omega\tau_j)}\right]. \tag{35}$$

Equation (35) may also be obtained from the general stress–strain relation by taking the Fourier transform $\int_{-\infty}^{+\infty}\langle\cdot\rangle\exp(i\omega t)dt$.

We use viscoelasticity data measured for the material similar to latex used in our experiments.[17] Instead of Eq. (35), this requires use of

$$E(\omega) = E - \sum_{j=1}^{N} \frac{i\omega\tau_j E_j}{(1 - i\omega\tau_j)}, \tag{36a}$$

$$E = \hat{E} - \sum_{j=1}^{N} E_j \quad \text{and} \quad E_j = \hat{E}\hat{E}_j, \tag{36b}$$

where the Young's modulus E corresponds to the equilibrium state and values of E_j and τ_j are taken for an elastomer with properties similar to latex,[17] see Table I. Note that modulus E is always set to 1.75 MPa.

In Fig. 5(a) the viscoelastic effect is illustrated. The assumed configuration is identical to that used in the experiments described in Sec. III. The results are computed in terms of insertion loss (IL) defined as

J. Acoust. Soc. Am., Vol. 128, No. 6, December 2010

Krynkin *et al.*: Periodic array of elastic shells   3501

TABLE I. Relaxation times and elastic moduli used in the definition of dynamic Young's modulus [Eq. (36)].

Relaxation time, τ_j (s)	Moduli, E_j (N/m²)
4.32×10^{-9}	9.00×10^6
5.84×10^{-8}	4.20×10^6
3.51×10^{-7}	2.94×10^6
2.28×10^{-6}	2.41×10^6
1.68×10^{-5}	1.87×10^6
2.82×10^{-4}	1.31×10^6
7.96×10^{-3}	7.02×10^5
9.50×10^{-3}	4.45×10^5

$$\text{IL} = 20 \log_{10} \left| \frac{H_0^{(1)}(k_o r)}{p_o} \right|. \qquad (37)$$

It is observed that the axisymmetric resonance discussed in Sec. II B is almost at the same frequency for both visco- and elastic solids, whereas the resonance related to indices $n = \pm 1$ is shifted to the higher frequency for the viscoelastic case. The slight shift in axisymmetric resonance gives better agreement with the data in Fig. 5(b). We also note the peak around 500 Hz is associated with the resonance of index $n = \pm 1$.

D. Array of elastic shells

We next consider finite array of thin elastic shells distributed in lattice with square cells of size L. Assuming that cylindrical source generates sound waves and using a multiple scattering technique,[2] the solution in the outer acoustic environment can be derived in the following form:

$$p_o(r, \theta) = H_0^{(1)}(k_o r) + \sum_{m=1}^{M} \sum_{n=-\infty}^{+\infty} A_n^m Z_n^m H_n^{(1)}(k_o \hat{r}_m) \exp(in\hat{\theta}_m), \qquad (38)$$

where M is the number of scatterers in the array, the first sum is taken over all numbers of shells in the array, the factors Z_n^m take the previously derived form (29) specified to the scatterer with index m, and variables $\hat{r}_m(r, \theta)$ and $\hat{\theta}_m(r, \theta)$ are the polar coordinates with origin in the center of shell of index m. Note that the solutions for the shells and the inner acoustic medium are identical to those in Sec. II B.

To compute the unknown coefficients A_n^m in Eq. (38), we again need to express solution (38) in terms of one set of polar coordinates $(\hat{r}_m, \hat{\theta}_m)$ that results in

$$\begin{aligned} p_o(\hat{r}_m, \hat{\theta}_m) = \sum_{n=-\infty}^{+\infty} & \{ J_n(k_o \hat{r}_m) H_n^{(1)}(k_o Q_m) e^{-in(\pi + \alpha_m)} \\ & + A_n^m Z_n^m H_n^{(1)}(k_o \hat{r}_m) + \sum_{p=1, p \neq m}^{M} \sum_{q=-\infty}^{+\infty} A_q^p Z_q^p J_n \\ & \times (k_o \hat{r}_m) H_{q-n}^{(1)}(k_o Q_{mp}) e^{i(q-n)(\pi + \alpha_{mp})} \} \\ & \times e^{in\hat{\theta}_m}, \quad m = 1, \dots, M, \end{aligned} \qquad (39)$$

where vector $\boldsymbol{Q}_m = Q_m(\cos \alpha_m, \sin \alpha_m)$ is the radius vector to the center of scatterer C_m and vector $\boldsymbol{Q}_{mp} = Q_{mp}(\cos \alpha_{mp}, \sin \alpha_{mp})$ defines the position of scatterer C_p with respect to scatterer C_m.
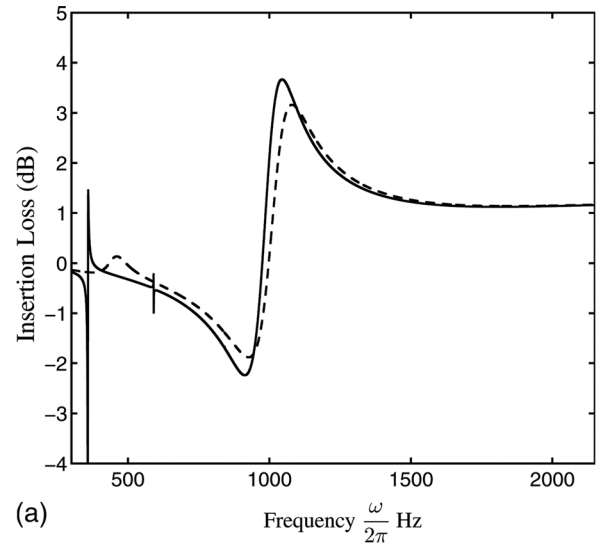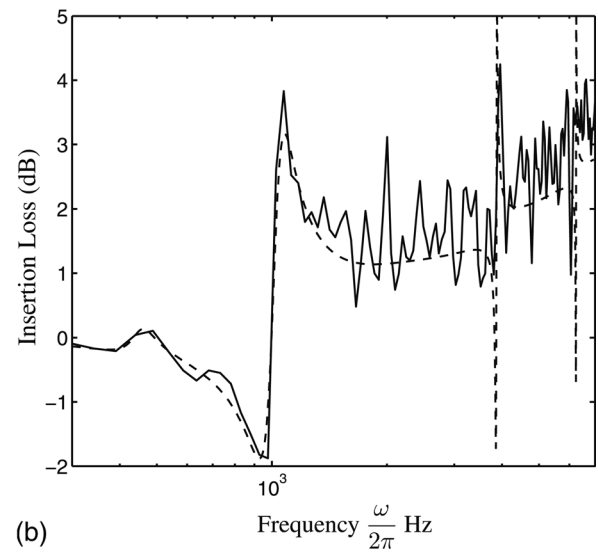
FIG. 5. IL computed and measured experimentally for single elastic shell made of latex. Distances from scatterer to the source and receiver are 1.5 and 0.05 m, respectively. The elastic shell is of radius 0.0275 m with thickness 0.00025 m. The experiments carried out to obtain these data are described in Secs. III A and III B. (a) Semi-analytical results for (——) elastic and (- - -) viscoelastic solids. (b) Data (——) compared with semi-analytical results (- - -) for a viscoelastic solid.

Use of the modified solution (39) in Eqs. (18) and (20) together with the solutions of inner acoustic medium and elastic shell makes it possible to derive the system of algebraic equations, which is similar to the one in Ref. 2, Eq. (4). This gives

$$\begin{aligned} A_n^m + \sum_{p=1, p \neq m}^{M} \sum_{q=-N}^{N} A_q^p Z_q^p H_{q-n}^{(1)}(k_o Q_{mp}) e^{i(q-n)(\pi + \alpha_{mp})} \\ = -H_n^{(1)}(k_o Q_m) e^{-in(\pi + \alpha_m)}. \end{aligned} \qquad (40)$$

The obtained algebraic system must be truncated to the finite number $M(2N + 1)$ of equations,[18] and then can be used to obtain the coefficients A_n^m, $n = 1, \dots, N$, $m = 1, \dots, M$ numerically.

Figure 6 illustrates results for the doubly periodic infinite array and its finite counterpart. The dimensions are taken from the results of Sec. II B. As expected the gaps between
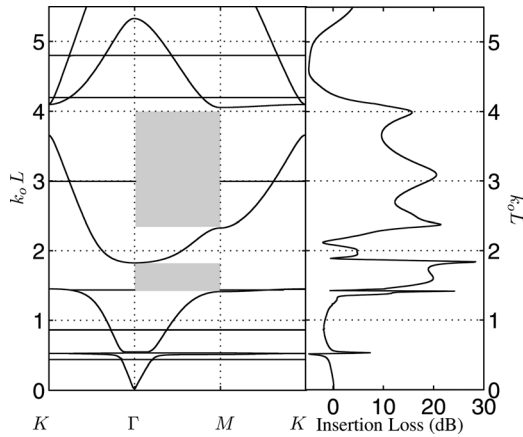
FIG. 6. The eigenvalue solution for the doubly periodic array of elastic shells and the corresponding prediction of IL for a finite array of 7×3 shells. The shaded areas indicate potentially useful bandgap regions.

the eigenvalue solutions correspond to the maxima of IL. In particular we are interested in the two shaded bandgaps.

The source and receiver are positioned along the line perpendicular to the longest axis of the finite array. This means that in the eigenvalue problem waves propagate along interval GM and the band diagram of this interval is compared with the computed IL. It is clearly seen that the shaded part of the bandgap related to the axisymmetric resonance is identified by a broad positive IL peak. Similarly the first and higher orders Bragg bandgaps can also be associated with positive IL peaks.

To compare the semi-analytical results with data, we again introduce viscoelasticity defined by a Young's modulus of complex form (36). This leads to redefining unknown coefficients in Eq. (39) by solving system (40) with modified elastic parameters. In Fig. 7(a) the theoretical predictions show relatively good agreement with data obtained for 7×3 array of elastic shells with lattice constant $L = 0.08$ m. Around 2000 Hz one can observe the effect of the periodic structure defined through the Bragg resonance that is

$$f = \frac{c_o}{2L} \text{ Hz.} \qquad (41)$$

The first and broad third peaks in the experimental results at 500 and 1200 Hz, respectively, can be identified as the results of the resonant behavior of the elastic shells. Since the resonance of index $n = \pm 1$ is dependent on polar angle, the small discrepancy in amplitude between theoretical and experimental results for the first peak may be explained by differences from the assumed source and receiver positions in the experiments. Due to the low-frequency regime, choice of more precise viscoelasticity parameters may also contribute to better agreement with the experiment for this particular resonance. The second peak at 750 Hz observed in the experiment can be explained by the presence of the resonance with index $n = \pm 2$. In the theoretical predictions where shell is homogeneous this resonance is almost negligible. However its contribution is predicted to be substantial if the elastic shell model is modified to include relatively stiff strips (modeled as rigid) and if the ideal cylindrical shape is slightly deformed. These modifications are pursued in Sec. III C. This model is closer to the cylindrical forms that result from the method of manufacture of the cylinders used in the experiments described in Sec. III.

Similar results depicted in Fig. 7(b) are obtained for bigger lattice constant $L = 0.1$ m. By changing size of the lattice cell, the frequencies of shell resonances are clearly not affected though the size of the associated IL peaks varies. As predicted by Eq. (41), we expect a shift in the position of the Bragg resonance that results in a new position of the associated IL peak.

III. MEASUREMENTS

A. Cylinders and support system

Latex sheets 2 m long and 0.25 m thick have been formed into cylinders with outer diameters of 27.5 and 55 mm, respectively. This has been achieved by overlapping
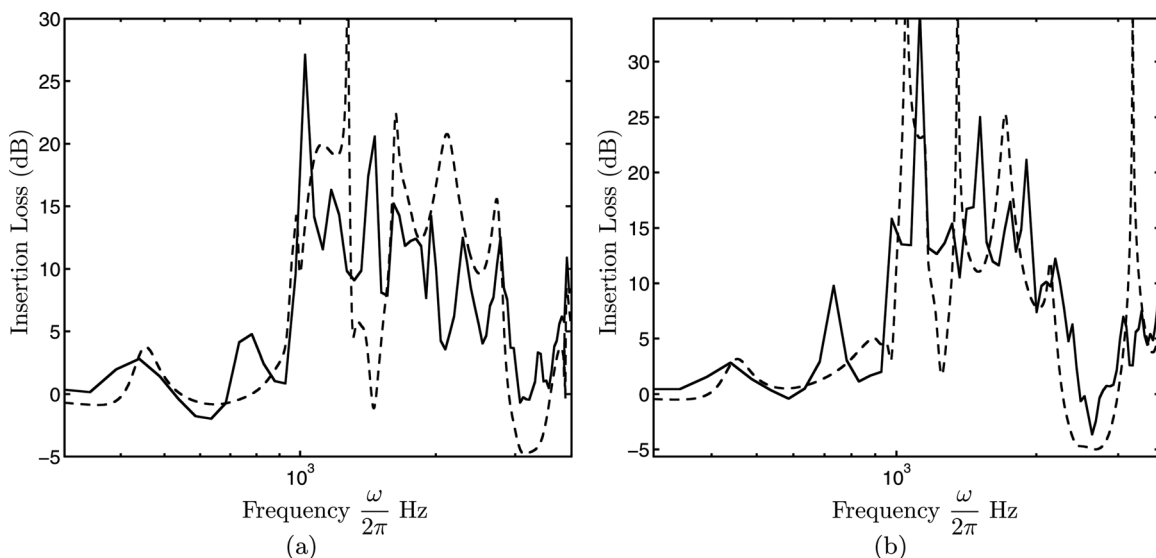

FIG. 7. IL spectra computed and measured experimentally for an array of 7×3 elastic shells. Distances from scatterer to the source and receiver are 1.5 and 0.05 m, respectively. The elastic shells are of radius 0.0275 m and thickness 0.00025 m. Data (——) are compared with semi-analytical results (- - -) for visco-elastic shell material. The experiments carried out to obtain these data are described in Secs. III A and III B. (a) $L = 0.08$ m; (b) $L = 0.1$ m.
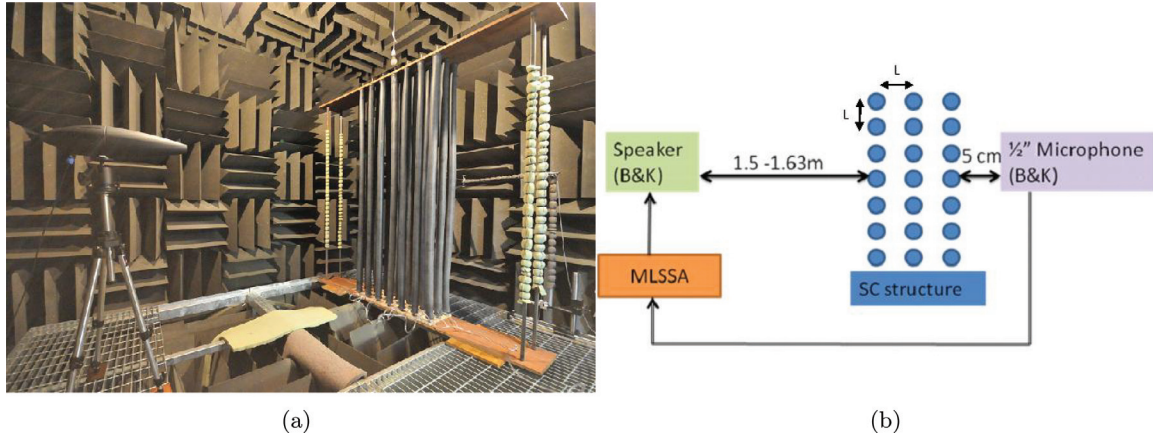
FIG. 8. (Color online) (a) 7 × 3 array of latex cylinders in the anechoic chamber; (b) plan of source, receiver, and array.

edges by a few millimeters and gluing them together. Supports for the 2 m long cylinders were provided by holed wooden boards at the top and base of each array [see Fig. 8(a)]. The lattice constant for the arrays of latex cylinders was 80 mm. To maintain their shape and vertical orientation, the latex cylinders were slightly inflated above atmospheric pressure through a common pipe connecting to a small pump. However deviations from the cylindrical shape were likely and could not be avoided.

B. Measurement system and data analysis

The sound source was a Bruel & Kjaer point source loudspeaker controlled by a maximum-length sequence system analyzer (MLSSA) system thus enabling determination of impulse responses. Measurements were taken from the IL spectra for single cylinders and arrays of cylinders in an anechoic chamber. Figures 8(a) and 8(b) show an example measurement arrangement. During the array measurements, the receiver microphone was positioned 50 mm from the nearest face of the array but on the opposite side to the source. Both source and receiver were 1.2 m above the floor of the chamber. The loudspeaker was placed between 1.5 and 1.63 m away from the array, such that the source–receiver axis was normal to the array orientation [see Fig. 8(b)]. IL spectra were calculated by subtracting signals received without and with the cylinder array present but with the support structure in place on both occasions.

C. Effect of gluing on the resonances of the shell

The elastic shell with glued section has non-uniform surface. This may have a significant effect on the performance of the SC composed of these shells. In order to study this effect the shell is modeled in COMSOL Multiphysics 3.4 as an elastic material with rigid strips that approximates the overlapping glued edges of the elastic sheet. The finite element (FE) simulation is defined by the quadratic elements and the active domain is meshed by at least five elements per wavelength. The numerical results have been obtained on a Dell workstation with 8 × Intel E430 processors and 32 GB random access memory (RAM). The estimated computational

time for solving the full problem in the frequency interval (0, 3000) Hz is 2 h.

Figure 9 illustrates the geometry used in the 2D numerical simulation. A rigid inclusion of width l has Neumann boundary conditions imposed at the acoustic interface and fixed faces (zero displacements) at the elastic interface. The elastic shell is modeled in a manner similar to that considered in the previous sections. As before the viscoelasticity is described by the dynamical Young's modulus given by relation (36) and Table I. Also it should be noted that the source is assumed to be an incident plane wave $\exp(ikx)$ propagating parallel to the Ox axis. However at the source–scatterer distances of interest, this is likely to give similar results to a point source. Note that some inaccuracy is expected below 500 Hz where the source–scatterer distance does not exceed three wavelengths.

In the formulation of the COMSOL model, the boundary conditions imposed on the surface of the elastic shell are similar to those in Eq. (5). The outer environment is surrounded by perfectly matched layers (PML) that replace the radiation condition (26). With PML boundaries and approximation of the point source by incident plane waves, the area
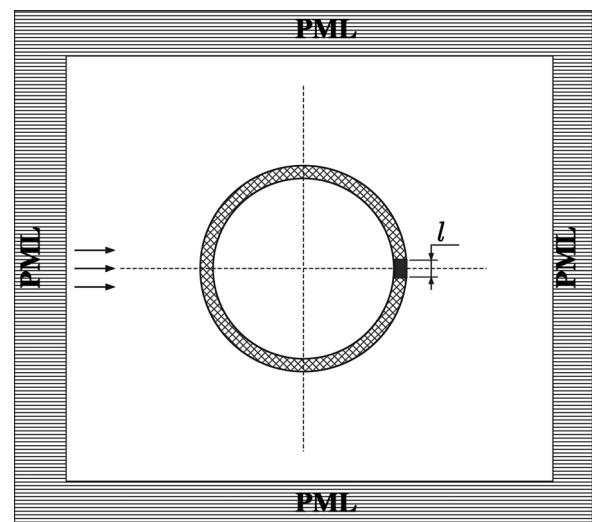

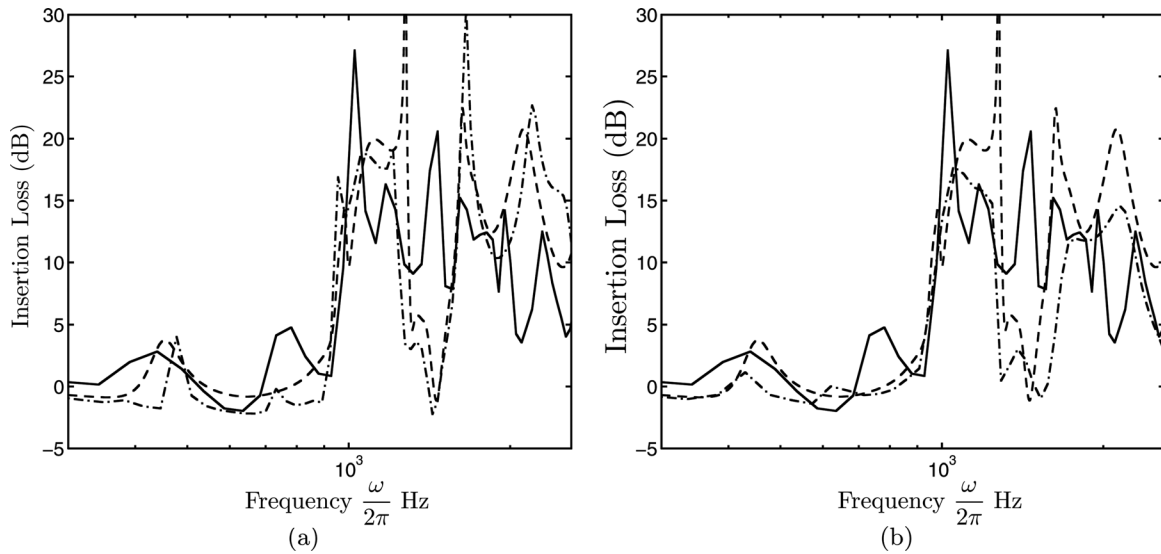FIG. 9. Cross-section of elastic cylindrical shell with rigid inclusion.

FIG. 10. ILs computed with FEM at the point $(L + 0.05 + b, 0)$ m $(-\cdot\cdot)$ compared with data (——) and semi-analytical results (- - -) for arrays of 7×3 cylindrical scatterers with lattice constant $L = 0.08$ m. Elastic shells used in FEM calculations have rigid inclusions of width $l = 0.01$ m. (a) $a_o = 0.0275$ m and $2h = 0.00025$ m; (b) $a_{o,1} = 0.032$ m, $a_{o,2} = 0.0221$ m, and $2h = 0.00025$ m.

of the outer domain in finite-element method (FEM) can be reduced to the size related to the array–receiver distance.

In Fig. 10(a) the performance of a 7×3 array of modified latex shells is compared with the results obtained in Sec. II D. It is shown that rigid inclusion of the given size has little impact on the positions of all three resonance frequencies of the elastic shell ($n = 0$, $n = \pm 1$, and $n = \pm 2$). However, the third resonance $f \approx 750$ Hz with index $n = \pm 2$ is amplified and becomes more noticeable.

As well as non-uniform boundary conditions due to gluing, significant changes in the form of the second and third resonances can also be the result of departures of the cross-sectional shapes of the elastic shells from circular. Figure 10(b) shows numerical predictions for a 7×3 array of elliptical shells. The semi-major $a_{o,1}$ and semi-minor $a_{o,2}$ axes are calculated on the assumption that the circumference is the same as that of a circular cylinder of radius $a_o = 0.0275$ m. Although it has not been possible to reproduce the measured form of the third resonance around $f \approx 650$ Hz exactly, it is predicted that this peak will broaden if the elastic shells are elliptical rather than circular in cross-section.

IV. CONCLUSIONS

SCs composed of elastic shells have been considered. Additional low-frequency bandgaps are predicted in an infinite periodic structure formed by the thin elastic shells made of suitably soft rubber. The additional bandgap due to the axisymmetric resonance of the shell is predicted to be the widest among those generated by the shell resonances. Its lower bound is given by a simple relation between material and geometrical parameters of the shell. This relation is obtained by using asymptotic equations for the thin elastic isotropic cylindrical shell subjected to the membrane compression form of loading. It provides a tool for choosing the material as well as radius and thickness of the shell so that the first resonances are positioned below the first Bragg

bandgap of the array. Viscoelasticity effect has also been included into the final results and gives better agreement with the experiments.

The presented semi-analytical method offers a fast and reliable approach to solving the problem of scattering by an array of cylindrical elastic shells. The computational time required by this method is less than one tenth of that needed for traditional numerical methods such as FEM.

The predicted performance of arrays of elastic shells in the low-frequency range has been verified by laboratory experiments. Measured low-frequency peaks correspond to the bandgaps related to the first shell resonances with indices $n = 0$, $n = \pm 1$, and $n = \pm 2$.

Without some form of protection, arrays of latex cylinders would be impractical in outdoor environments. Therefore the acoustical effects of providing suitable protection are being investigated.

[1] T. Miyashita, "Sonic crystals and sonic wave-guides," Meas. Sci. Technol. **16**, 47–63 (2005).

[2] O. Umnova, K. Attenborough, and C. M. Linton, "Effects of porous covering on sound attenuation by periodic arrays of cylinders," J. Acoust. Soc. Am. **119**, 278–284 (2006).

[3] R. Sainidou, B. Djafari-Rouhani, Y. Pennec, and J. O. Vasseur, "Locally resonant phononic crystals made of hollow spheres or cylinders," Phys. Rev. B **73**, 024302 (2006).

[4] M. Hirsekorn, P. P. Delsanto, N. K. Batra, and P. Matic, "Modelling and simulation of acoustic wave propagation in locally resonant sonic materials," Ultrasonics **42**, 231–235 (2004).

[5] M. S. Kushwaha and P. Halevi, "Stop bands for cubic arrays of spherical balloons," J. Acoust. Soc. Am. **101**, 619–622 (1997).

[6] E. Fuster-Garcia, V. Romero-Garcia, J. V. Sánchez-Pérez, and L. M. Garcia-Raffi, "Targeted band gap creation using mixed sonic crystal arrays

J. Acoust. Soc. Am., Vol. 128, No. 6, December 2010

Krynkin *et al.*: Periodic array of elastic shells   3505

including resonators and rigid scatterers," Appl. Phys. Lett. **90**, 244104 (2007).

[7]X. Hu, C. T. Chan, and J. Zi, "Two-dimensional sonic crystals with Helmholtz resonators," Phys. Rev. E **71**, 055601(R) (2005).

[8]Z. Y. Cui, T. N. Chen, H. L. Chen, and Y. P. Su, "Experimental and calculated research on a large band gap constituting of tubes with periodic narrow slits," Appl. Acoust. **70**, 1087–1093 (2009).

[9]N. A. Nicorovici and R. C. McPhedran, "Photonic band gaps for arrays of perfectly conducting cylinders," Phys. Rev. E **52**, 1135–1145 (1995).

[10]G. C. Gaunaurd, "Sonar cross section of a coated hollow cylinder in water," J. Acoust. Soc. Am. **61**, 360–368 (1977).

[11]L. Rayleigh, "On the influence of obstacles arranged in rectangular order upon the properties of a medium," Philos. Mag. **34**, 481–502 (1892).

[12]A. B. Movchan, N. V. Movchan, and C. G. Poulton, *Asymptotic Models of Fields in Dilute and Densely Packed Composites* (Imperial College Press, London, 2002), pp. 143–151.

[13]C. G. Poulton, A. B. Movchan, R. C. McPhedran, N. A. Nicorovici, and Y. A. Antipov, "Eigenvalue problems for doubly periodic elastic structures and phononic band gaps," Proc. R. Soc. London, Ser. A **456**, 2543–2559 (2000).

[14]J. D. Kaplunov, L. Yu. Kossovich, and E. V. Nolde, *Dynamics of Thin Walled Elastic Bodies* (Academic Press, London, 1998), p. 110.

[15]M. Abramowitz and I. A. Stegun, *Handbook of Mathematical Functions* (National Bureau of Standards, Washington, D.C., 1964), p. 255.

[16]I. N. Sneddon and R. Hill, *Progress in Solid Mechanics*, Vol. I (North-Holland Publishing Company, Amsterdam, 1960), pp. 4–11.

[17]B. Merheb, P. A. Deymier, M. Jain, M. Aloshyna-Lesuffleur, S. Mohanty, A. Berker, and R. W. Greger, "Elastic and viscoelastic effects in rubber-air acoustics band gap structures: A theoretical and experimental study," J. Appl. Phys. **104**, 064913 (2008).

[18]C. M. Linton and D. V. Evans, "The interaction of waves with arrays of vertical circular cylinders," J. Fluid Mech. **215**, 549–569 (1990).